ACS NANO

www.acsnano.org

ARTICLE

Natural-Wood-Inspired Ultrastrong Anisotropic Hybrid Hydrogels Targeting Artificial Tendons or Ligaments

Lu Wu,[‖] Yue Kang,[‖] Xiaoyu Shi, Bin Yuezhen, Meijie Qu, Jianyi Li, and Zhong-Shuai Wu*

Cite This: *ACS Nano* 2023, 17, 13522–13532

Read Online

ACCESS | Metrics & More | Article Recommendations | Supporting Information

ABSTRACT: **Hydrogels are able to mimic the flexibility of biological tissues or skin, but they still cannot achieve satisfactory strength and toughness, greatly limiting their scope of application. Natural wood can offer inspiration for designing high-strength hydrogels attributed to its anisotropic structure. Herein, we propose an integrated strategy for efficient preparation of ultrastrong hydrogels using a salting-assisted prestretching treatment. The as-prepared poly(vinyl alcohol)/cellulose nanofiber hybrid hydrogels show distinct wood-like anisotropy, including oriented molecular fiber bundles and extended grain size, which endows materials with extraordinarily comprehensive mechanical properties of ultimate breaking strength exceeding 40 MPa, strain approaching 250%, and toughness exceeding 60 MJ·m^{-3}, and outstanding tear resistance. Impressively, the breaking strength and toughness of the reswollen preoriented hydrogels approach 10 MPa and 25 MJ·m^{-3}, respectively. *In vitro* and *in vivo* tests demonstrate that the reswollen hydrogels do not affect the growth and viability of the cells, nor do they cause the inflammation or rejection of the mouse tissue, implying extremely low biotoxicity and perfect histocompatibility, showcasing bright prospects for application in artificial ligaments or tendons. The strategy provided in this study can be generalized to a variety of biocompatible polymers for the fabrication of high-performance hydrogels with anisotropic structures.**

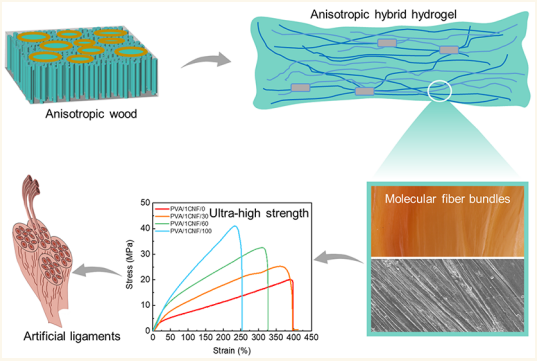

KEYWORDS: *Hydrogel, High strength, Orientation, Cellulose nanofiber, Hybrid*

INTRODUCTION

Hydrogels can perfectly simulate natural tissues and are considered as viable candidates for biomedical and bioengineering applications such as soft actuators,[1] artificial muscles,[2] and artificial ligaments,[3] due to their 3D network structure, ideal flexibility, and water content similar to that of biological tissue. Further, the abundant ions in hydrogels ensure their wide application in energy storage.[4,5] A series of natural-polymer-based hydrogels prepared by Hu's group offered surprising electrochemical behavior for use in Zn batteries.[6−8] Unfortunately, most of the hydrogels demonstrate low tensile strength and are easily damaged, seriously limiting their further applications.[9,10] Recently, several key strategies have been developed for the fabrication of high-strength hydrogels, mainly through construction of dual networks,[11,12] compositing of nanomaterials,[13,14] and synergy of multiple interactions.[15] The hydrogels constructed by these methods exhibit improved mechanical strength, but despite this, the material still has difficulty reaching a breaking strength of 10 MPa.

Natural wood is both strong and light, which allows its usage for a range of constructions, and has a profound impact on human life.[16] The broad range of applications of natural wood benefits from its outstanding comprehensive properties, including low density, impressive strength, and high toughness,[17,18] arising from its anisotropic structure.[19] The oriented arrangement of numerous fibers consisting of lignin, cellulose, and hemicellulose contributes decisively to the extremely good mechanical strength.[20] Similarly, some human tissues, such as muscles and ligaments, also display a highly parallel-aligned fibrous structure that endows the tissue with unparalleled mechanical strength and toughness, ensuring a life full of vigor and vitality in various organisms.[21,22] Therefore, it is deduced that creating highly ordered structures in hydrogel networks using appropriate strategies would be an effective way to obtain

Received: March 2, 2023
Accepted: July 12, 2023
Published: July 13, 2023

https://doi.org/10.1021/acsnano.3c01976
ACS Nano 2023, 17, 13522−13532

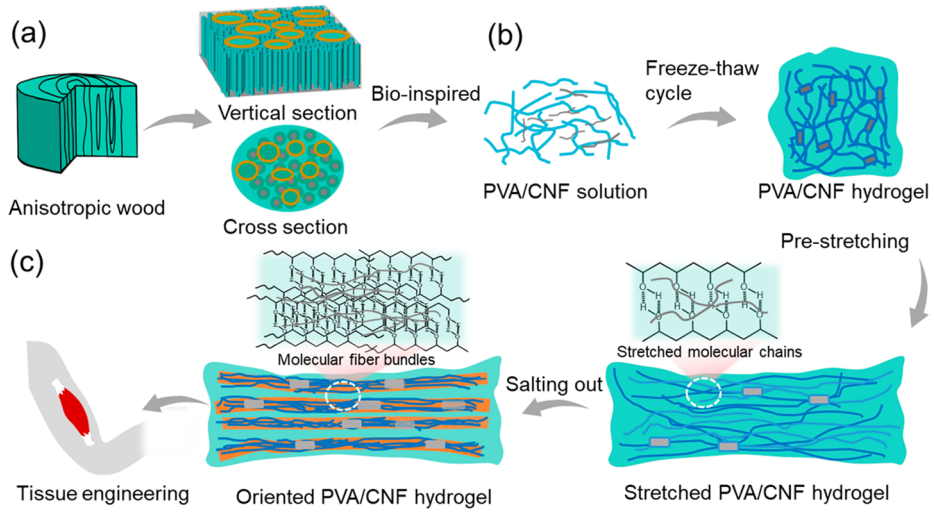

Figure 1. Schematic illustration of fetching to the PVA/CNF hydrogel. (a) Anisotropic structure of wood. (b) Preparation process of the PVA/CNF hydrogel (freeze−thaw cycle). (c) Preparation method and internal structure of oriented PVA/CNF.

high-strength hydrogels. Recently, methods to prepare anisotropic hydrogels with oriented structures and improved mechanical performance have been reported.[23,24] Among them, the wood template method has provided hydrogel products with superior strength (>20 MPa) and perfectly oriented structure.[25,26] For example, lignin in wood can be removed with oxidizing agents to create directionally aligned channels. These channels can be completely filled with hydrophilic polymers, such as polyacrylamide or poly(vinyl alcohol) (PVA), and form a strong composite hydrogel with cellulose bundles. The breaking strength of these composite hydrogels can easily reach or exceed 20 MPa due to the directionally aligned cellulose fibers. However, the elongation at break of such composite hydrogels hardly exceeds 50% due to the inherent rigidity of the cellulose bundles, resulting in a poor toughness.[25,27] Therefore, it is still a far-reaching and challenging endeavor to develop a reasonable strategy to accomplish the preparation of a hydrogel with both strong strength and high toughness.

Some salt solutions can significantly enhance the interaction between macromolecular chains and transform them to a tighter, more stable aggregated state via a salting-out-induced process,[28] which is known as the Hofmeister effect.[29] This behavior is dominated by anions, and the precipitation ability of different anions to macromolecular chains is ordered as $CO_3^{2-} > SO_4^{2-} > S_2O_3^{2-} > H_2PO_4^- > F^- > CH_3COO^- > Cl^- > Br^-$.[30] In addition, the stress stretching process can induce directional alignment of molecular chains and endow hydrogels with anisotropic structures, which can also improve the mechanical performance of the material. Herein, taking inspiration from natural wood, we develop a type of anisotropic poly(vinyl alcohol)/cellulose nanofiber (PVA/CNF) hybrid hydrogel by combining salting-out treatment with a preorientation strategy. The PVA with a large number of hydroxyl groups could be easily transformed into a gel state and smoothly form a large number of strong hydrogen-bonding cross-linking points with CNF. Fixation of the prestretched hydrogel molecular chains by the salt solution was applied to achieve a stable anisotropic oriented structure and to obtain exceptional mechanical properties of ultrahigh breaking strength (~40 MPa) and ideal toughness (~60 MJ·m^{-3}). Contrary to the reported oriented wood hydrogels, the main body and backbone of PVA/CNF hydrogels were the flexible PVA molecular chains rather than the nonstretchable, directionally aligned natural wood fibers, offering a high elongation at break of the material. Moreover, the fully swollen hydrogels still maintained satisfactory mechanical properties, including strong strength and high toughness, and showed little cytotoxicity, which was a prerequisite for their application in both artificial ligaments and muscles.

RESULTS AND DISCUSSION

Figure 1 depicts the clear anisotropic structure of wood and the manufacturing and preparation processes of oriented PVA/CNF hybrid hydrogels. Through a combined prestretching−salting-out fixation strategy, the randomly oriented PVA molecular chains underwent sufficient alignment while the salt solution fixed the oriented molecules and formed stronger molecular bundle fibers together with the CNF. Briefly, the PVA/CNF mixture solution was converted to a gel state by a simple freeze−thaw cycle. The hydrogel was then prestretched and fixed, followed by complete immersion in sodium sulfate solution. The free PVA molecular chains and CNF were oriented under tensile stress, and the degree of molecular chain orientation could be well controlled by deformation variables. Subsequently, large amounts of ions could induce the deposition and aggregation of oriented polymer molecules, which led to the formation of thick bundles of PVA/CNF molecular fibers. Both the salting-out treatment and CNF can change the mechanical properties of hydrogels to some extent. As shown in Figure S1, the breaking strength of PVA hydrogels subjected to one freeze−thaw cycle was only 200 kPa, and the breaking strength of the hydrogels increased significantly with a longer soaking time, finally reaching 6.4 MPa after 24 h of soaking. By continuously increasing the soaking time, the breaking strength of the PVA hydrogel no longer increased significantly; therefore, 24 h was determined as the optimal soaking time. Subsequently, the CNF was introduced into the PVA hydrogel to investigate its effect on the mechanical properties of the material. It is clearly found that the breaking strength of PVA hydrogels showed a volcano-like trend as the CNF content increased, and 1 wt% CNF resulted in the optimal comprehensive mechanical properties (Figure S2). This is mainly because CNF has a large aspect ratio (Figure

https://doi.org/10.1021/acsnano.3c01976
ACS Nano 2023, 17, 13522−13532

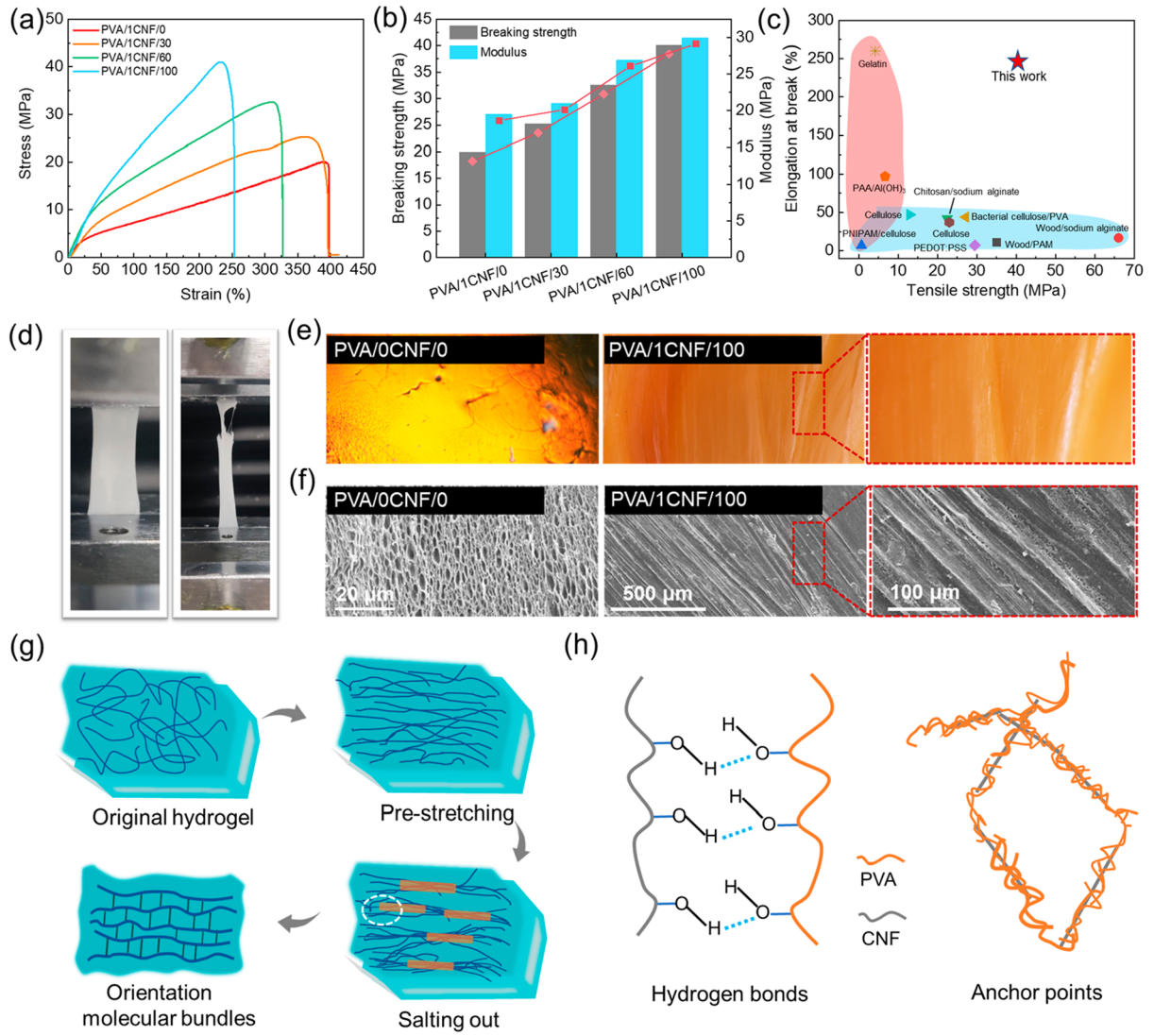

Figure 2. (a) Stress−strain curves of PVA/1CNF/*y* hydrogels with different prestretched deformation variables. (b) Breaking strength and modulus of PVA/1CNF/*y* hydrogels with different prestretched deformation variables. (c) Elongation at break and breaking strength of strong hydrogels in some representative literature reports. (d) Digital photos of anisotropic PVA/1CNF/100 hydrogel in original and fractured states. (e) Optical micrograph of the original PVA hydrogel and anisotropic PVA/1CNF/100. (f) SEM images of the original PVA hydrogel and anisotropic PVA/1CNF/100 hydrogel. (g) Schematic diagram of the change in the molecular chain during the preparation of anisotropic PVA/1CNF/100 hydrogel. (h) Interaction between CNF and PVA molecular chains.

S3) and a large number of hydroxyl groups which enhance intermolecular interactions (hydrogen bonds and molecular entanglement), thereby improving the strength of the hydrogel.[31] This is widely known as the nanoenhancement effect of CNF. The slight decrease in breaking strength due to high CNF content (1.2 wt%) may be caused by the imperfect dispersion of CNF, leading to an increase in microdefects within the hydrogel. Similarly, the mechanical properties of the PVA/CNF hydrogel were further improved after 24 h of soaking, and the hydrogel containing 1 wt% CNF (PVA/1CNF/0) could still exhibit a maximum breaking strength of about 20 MPa (Figure S4). More attractively, the orientation behavior pushes the mechanical properties of the hydrogels to an amazing level. From Figure 2a, the anisotropic PVA/CNF hydrogel constructed by this method displayed a breaking strength of more than 40 MPa and an elastic modulus of 30 MPa along the orientation direction. What's more, the elongation at break of the hybrid hydrogel exceeded 250% (Figure 2a,b), which was much higher than that of general wood-based high-strength hydrogels (<20%).[25,32] The breaking strength and modulus of anisotropic PVA/CNF hydrogels showed a clearly positive correlation with the prestretching deformation. Compared to the unstretched treated samples, the 30% prestretched samples (PVA/1CNF/30) resulted in a hydrogel strength of 25.3 MPa with a 26% improvement in strength. The breaking strength of the hydrogel exceeded 40 MPa when the prestretch deformation was expanded to 100% (PVA/1CNF/100), witnessing a change of 110%. Moreover, the PVA/1CNF/100 anisotropic hydrogel presented a high toughness of 61.8 MJ·m^{-3}. These surprisingly high values far exceed the values in the relevant works (Figure 2c).[9,25,32−39] Macroscopically, the anisotropic PVA/1CNF/100 hydrogel had the appearance of a white opaque solid, resulting from the combined effect of the salt solution and prestretching. In the prestretching process, the curled macromolecular chains were gradually transformed into a directionally stretched state.

https://doi.org/10.1021/acsnano.3c01976
ACS Nano 2023, 17, 13522−13532

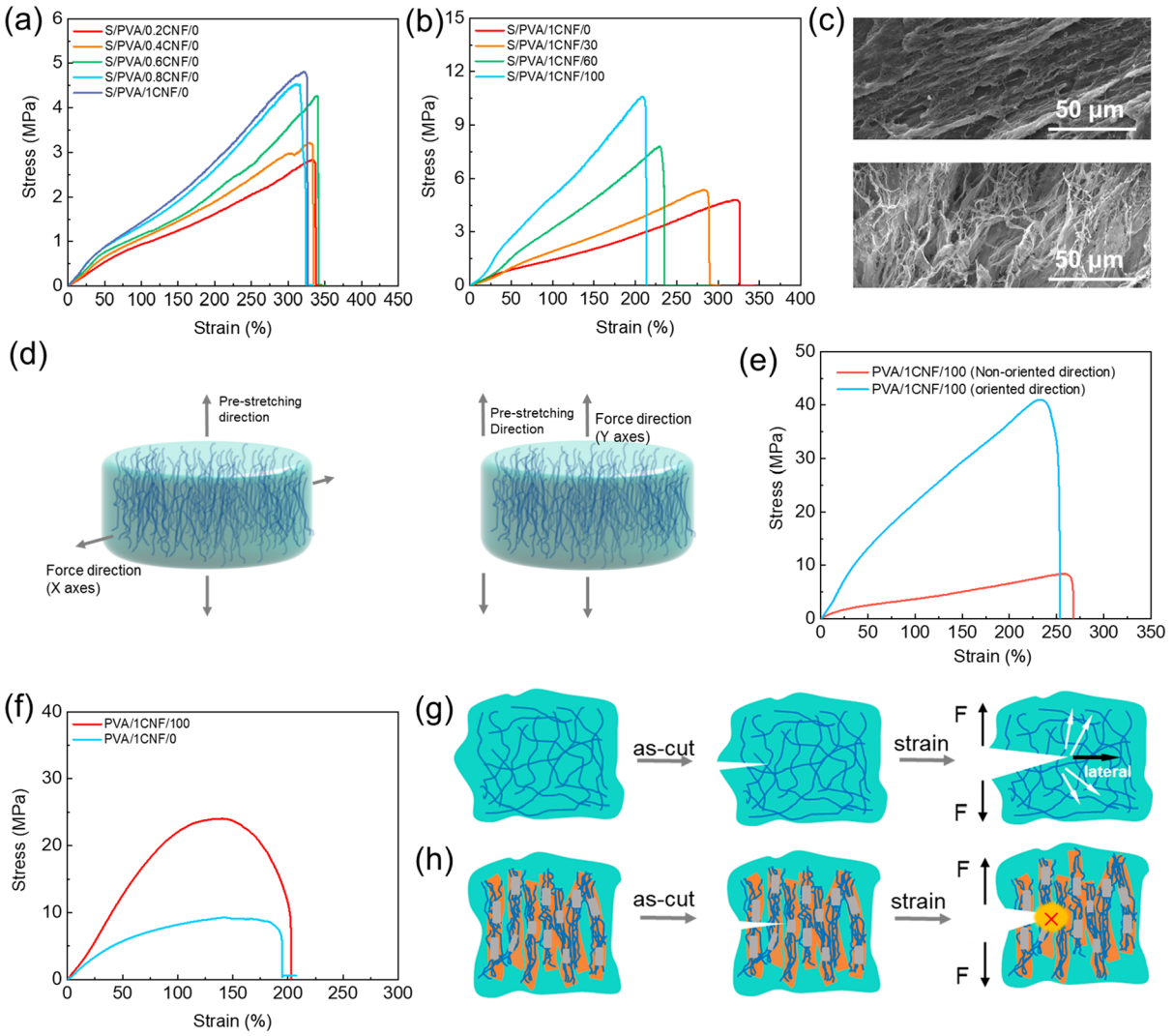

Figure 3. (a) Stress−strain curves of S/PVA/*x*CNF/0 hydrogels with different CNF contents. (b) Effect of prestretching behavior on the mechanical properties of S/PVA/1CNF/*y* hydrogels with different prestretch deformation variables. (c) SEM images of the S/PVA/1CNF/100 hydrogel. (d) Schematic diagram of the stretching experiment in the oriented and nonoriented directions. (e) Stress−strain curves of anisotropic PVA/1CNF/100 hydrogel along both oriented and nonoriented directions. (f) Notch test stress−strain curve of original and anisotropic hydrogels. (g, h) Schematic diagrams of notch expansion during stretching of original PVA/1CNF/0 (g) and anisotropic PVA/1CNF/100 (h) hydrogels.

Meanwhile, the CNFs were entangled and wrapped by PVA molecular chains to form anchor points, which further facilitated the directional stretching of macromolecules during the prestretching process. Subsequently, the salt solution induced hydrophobic aggregation of the oriented macromolecular chains, which contributed to the formation of oriented molecular fibrils and caused the transition from translucent to white opaque hydrogels.[37,40] Notably, the tensile fracture showed a clear fibrous morphology (Figure 2d), which could be proven by the SEM image of the fracture section (Figure S5), indicating the formation of a large number of oriented macromolecular bundles inside the hydrogel. The original PVA hydrogel (PVA/0CNF/0) (Table S1) had a homogeneous gel-like morphology, while the 100% prestretched hydrogel (PVA/1CNF/100) exhibited a distinctly oriented arrangement of fibrous structures inside (Figure 2e). The large difference in SEM images likewise confirmed the phenomenon of oriented alignment of macromolecular chains within the hydrogel. After freeze-drying, the pristine PVA hydrogels showed a continuous and uniform porous network structure on the inside with no amorphization (Figure 2f). In contrast, the surface of PVA/1CNF/30 with 30% prestretching deformation emerged with characteristic directionally arranged wrinkles, implying the onset of formation of directional fiber bundles inside the hydrogel (Figure S6). As the prestretching deformation increased, the orientation structure became increasingly evident and the molecular fiber bundles were aligned more and more closely, gradually converging to the parallel state, which manifested that the macromolecules inside the hydrogel became more ordered (Figure S6). From the longitudinal cross-sectional SEM images, compactly arranged continuous fiber bundles could be observed more clearly, and their lengths exceeded 500 μm (Figure 2f), which was attributed to the ordered aggregation of a large number of PVA molecular chains. This distinct oriented structure shares striking resemblances with the internal structure of wood and

https://doi.org/10.1021/acsnano.3c01976
ACS Nano 2023, 17, 13522−13532

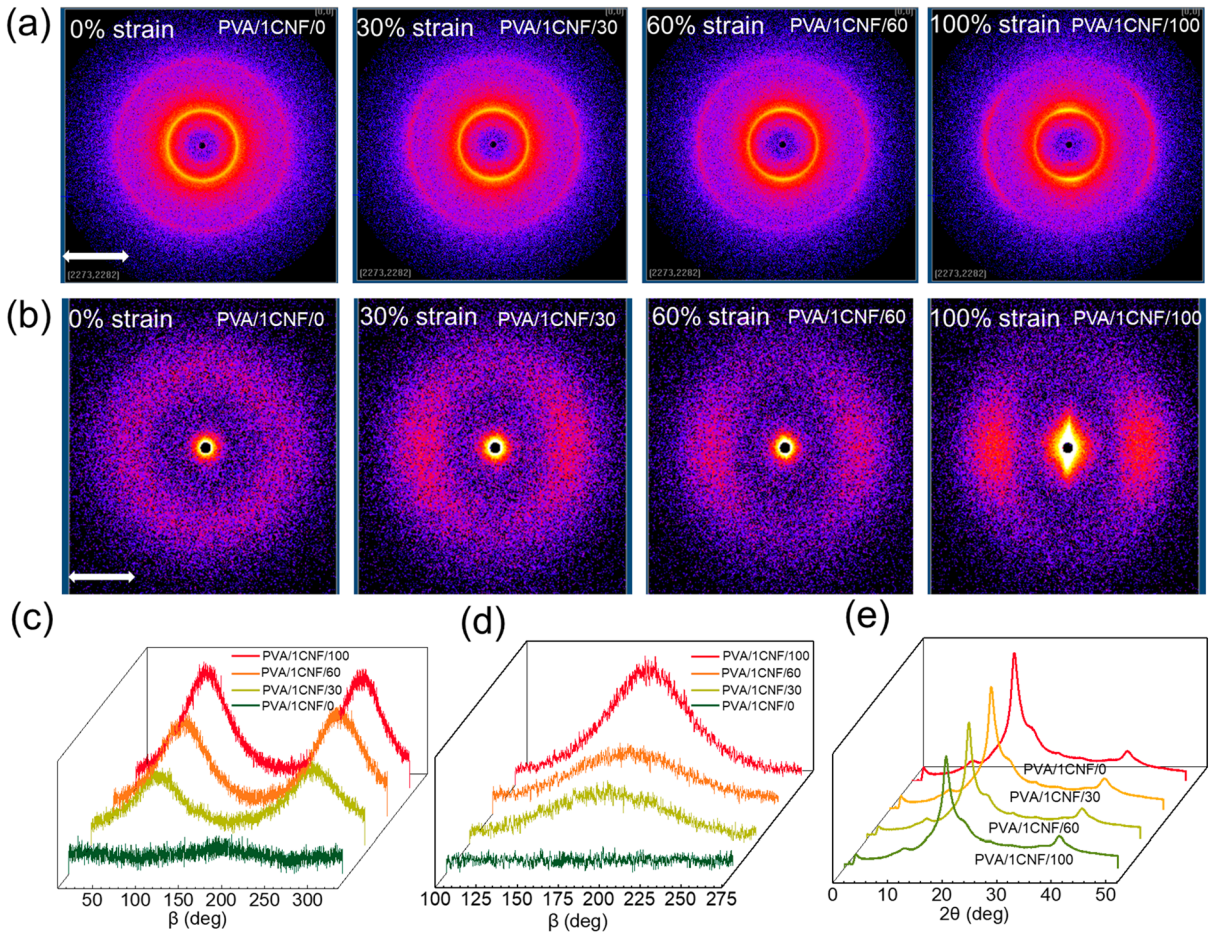

Figure 4. (a) 2D WAXD patterns of PVA/1CNF/*y* hydrogels with different prestretched deformation. (b) 2D SAXS patterns of PVA/1CNF/*y* hydrogels with different prestretched deformation. (c, d) Correlation of the azimuthally integrated intensity distribution of (c) 2D WAXD and (d) 2D SAXS patterns with prestretched deformation. (e) 1D WAXD profiles of different PVA/1CNF/*y* hydrogels.

supports the hydrogel's superior properties (Figure S7). The formation of molecular fiber bundles in hydrogels is described in Figure 2g. After the freeze−thaw cycle, the free molecular chains were partially immobilized by hydrogen bonding, leading to the conversion of the solution into a gel state. Also, the connection between CNF and PVA molecular chains became stronger because of the formation of hydrogen bonds (Figure 2h). Subsequently, during the prestretching process, the molecular chains in the hydrogel underwent directional alignment under the action of external forces. Most importantly, the salt solution could induce the aggregation of adjacent oriented macromolecules into bundles and immobilize them, causing the emergence of molecular fibers (Figure 2g). In this process, the CNF dispersed in the hydrogel could be regarded as anchor points, and a large number of PVA molecular chains would wrap around the CNF surface and form longer molecular nanofibers, which contributed to the increase in molecular fiber bundle aspect ratio (Figure 2h). We analyzed the effects of CNF introduction and preorientation effects on the internal molecular structure of the hydrogels using FTIR. The FTIR spectra of PVA, PVA/1CNF/0, and anisotropic PVA/1CNF/100 hydrogels are plotted in Figure S8. It can be seen that the PVA and PVA/1CNF/0 hydrogels show an obvious C−O stretching vibration absorption peak at 1100 cm^{-1}, a C−H stretching vibration absorption peak near 2950 cm^{-1}, and an O−H stretching vibration absorption peak at 3000−3400 cm^{-1}.[41−43] Importantly, there was no significant change in the peak positions among different samples, indicating that CNF and PVA were not connected by chemical bonds. However, the addition of CNF shifted the vibrational absorption peak of O−H in the material compared to the pure PVA hydrogel, demonstrative of the formation of hydrogen bonds between PVA and CNF.[44] Besides, the peak positions of the preoriented hydrogel did not move, manifesting that the prestretching treatment did not change the bonding structure inside the hydrogel.

The super swelling ability of a hydrogel, as a soft material, is the signature feature. A large amount of water enters the hydrogel network during the swelling process, leading to a sharp decrease in the mechanical properties of the hydrogel and hindering its application in tissue engineering. The salt-solution-soaked PVA/CNF hydrogels were put into deionized water to analyze the changes in mechanical properties of different samples after swelling. From Figure 3a, it was found that the reswollen hydrogels showed an unavoidable decrease in strength, with a maximum strength of 5 MPa for PVA/1CNT/0 hydrogels. In addition, the CNF content continued to influence the mechanical behavior of PVA/CNF hydrogels, and the breaking strength gradually increased with the increase in CNF content. In contrast, the prestretched samples after swelling exhibited significantly higher breaking strength and toughness. As seen in Figure 3b, the strength and toughness of

https://doi.org/10.1021/acsnano.3c01976
ACS Nano 2023, 17, 13522−13532

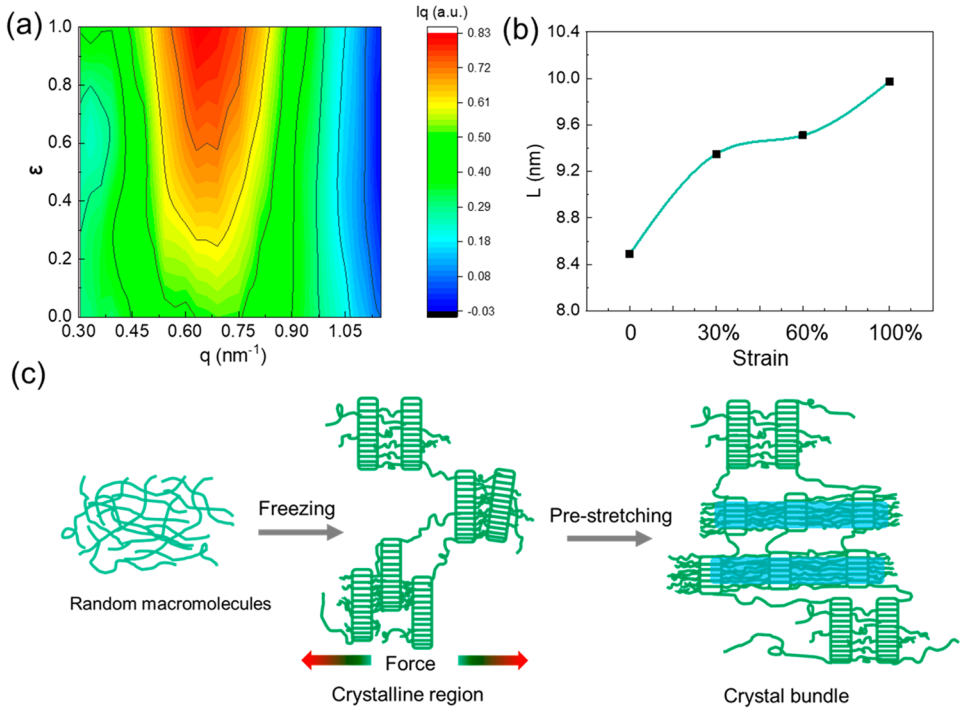

Figure 5. (a) Contour map of the 2D SAXS data, with colors indicating the scattering intensity in the equatorial direction. (b) Change of the long period of lamellar crystals with prestretching deformation. (c) Schematic diagram of the structural changes of PVA/1CNF/100 hydrogel during prestretching.

the reswollen anisotropic PVA/1CNF/100 hydrogel (S/PVA/1CNF/100) could still reach 10 MPa and 25.8 MJ·m^{-3}, respectively, which far superseded the unoriented sample. Microstructure analysis confirmed that the swollen anisotropic hydrogel appeared to have a distinctive porous-like structure, indicative of the expansion of the internal network. Importantly, the orientation structures inside the hydrogel did not disappear, which was responsible for maintaining the excellent mechanical properties (Figure 3c).

As with the wood, the mechanical behaviors of the anisotropic hydrogel were significantly different in the vertical and horizontal directions. To investigate the anisotropy of the mechanical properties, the anisotropic PVA/1CNF/100 hydrogel specimens were cut in the oriented and nonoriented directions, and the tensile strength of the prepared samples was measured. Clearly, the breaking strength and modulus of the anisotropic PVA/1CNF/100 hydrogel were 8.1 and 9.4 MPa in the nonoriented direction and 40.1 and 30.0 MPa in the oriented direction, respectively (Figure 3d,e and Figure S9). As expected, the breaking strength and modulus of the material in the oriented direction were significantly higher than the corresponding values in the nonoriented direction, which was a result of the oriented alignment of the molecular bundles. Impressively, even with pre-existing cracks, the anisotropic hydrogel of PVA/1CNF/100 could still reach an elongation at break of about 200%, which was nearly 78% of the elongation of intact samples. In contrast, although the elongation at break of the notched unoriented sample (PVA/1CNF/0) was also close to 200%, this value was only 52% of the elongation of the corresponding intact sample (Figure 3f). This result proved that the presence of the oriented structure could effectively improve the crack-blocking ability and tear resistance of the hydrogel. From a fracture perspective, disordered macromolecular chains wound around each other and prevented sliding between the polymer molecules, which resulted in a rapid expansion of energy dissipation radially throughout the whole network and certainly in the lateral direction of notch extension and deteriorated the rate of notch expansion (Figure 3g). In contrast, the large number of molecular fiber bundles inside the oriented hydrogel helps the gel resist stronger external stresses,[45,46] and in addition, sliding between oriented fiber bundles occurred more easily compared to that of disordered macromolecular chains wound around each other, which effectively slowed the rate of notch expansion and raised the tearing energy of the material (Figure 3h).

To confirm the orientation behavior of the macromolecules in the samples, 2D WAXD (Figure 4a) and 2D SAXS (Figure 4b) analyses were performed on the oriented and nonoriented hydrogels. To avoid signal interference from large amounts of sodium sulfate crystals, fixture-fixed hydrogels were first soaked with sufficient cold deionized water to remove sodium sulfate and then completely dried at 35 °C. From Figure 4a, the diffraction intensity of the original PVA/1CNF/0 hydrogel showed a clear isotropy. In contrast, the diffraction intensity of the prestretched samples (PVA/1CNF/30, PVA/1CNF/60, and PVA/1CNF/100) exhibited a significant anisotropy, and the regular diffraction rings gradually changed to diffraction arcs with the increase of prestretched deformation. Moreover, the azimuth angle of the hydrogel sample at 90° and 270° increased gradually with the prestretching deformation and became more and more sharp (Figure 4c). These clearly signaled the appearance of orientation alignment inside the hydrogel.[47] Further, the 2D SAXS pattern of the original PVA/1CNF/0 hydrogel was distinctly isotropic, as evidenced by the almost identical scattering intensity in all directions (Figure 4b). In contrast, the prestretched samples (PVA/1CNF/30, PVA/1CNF/60, and PVA/1CNF/100) exhibited an elliptical shape with a significantly stronger scattering signal along the

https://doi.org/10.1021/acsnano.3c01976
ACS Nano 2023, 17, 13522−13532

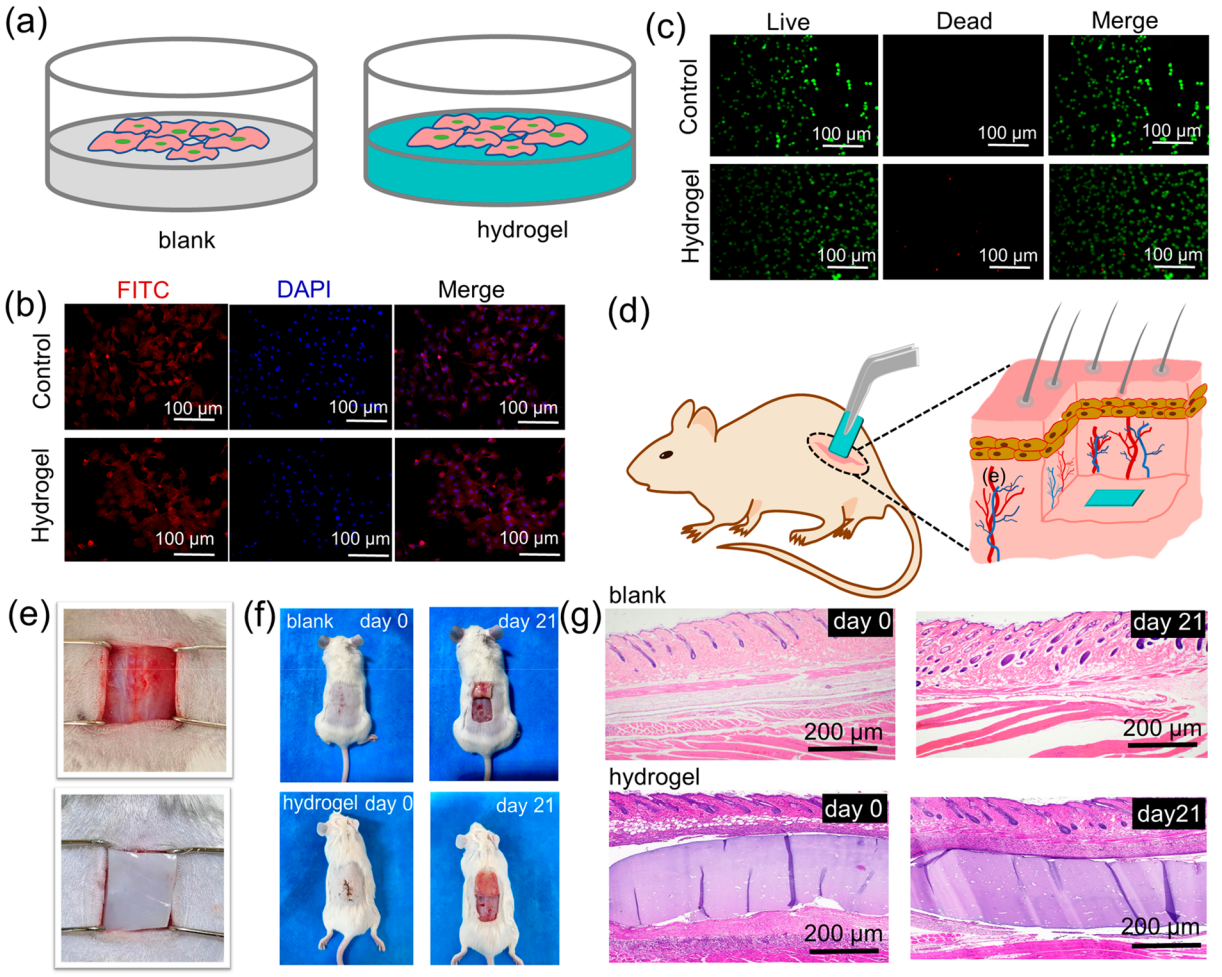

Figure 6. Biocompatibility assessment. (a) Cell culture on blank and hydrogel substrates. (b) Morphology of HUVECs on blank and hydrogel substrates. (c) Fluorescent images of live/dead assay after culturing HUVECs onto the hydrogel for 72 h. (d) Schematic diagram of the gel implantation process. (e) Digital photos of the hydrogel at the time of implantation. (f) Inflammation test involving implanting the hydrogel into mouse subcutaneous tissue. (g) Hematoxylin and eosin (H&E) staining after breeding for 0 and 21 days.

axis perpendicular to the stretching direction than parallel to the stretching direction, and the eccentricity of the spot increased with increasing prestretching deformation (Figure 4b). Figure 4d shows the azimuth angle integration curves (101 crystal planes) of the different 2D SAXS patterns. The azimuthal intensity located at 90° demonstrates a significant positive correlation with the prestretched shape deformation. Therefore, it is proved that when the hydrogel samples were stretched, the polymer molecular chains indeed underwent an oriented arrangement and formed anisotropic permanent structures in parallel to the stretching direction under the action of salting-out precipitation.

As seen in the 1D profile of 2D WAXD patterns (Figure 4e), the diffraction peaks at 11.2°, 18.6°, and 39.3° on the curves correspond to the 100, 101, and 111 crystal planes of PVA, respectively.[48] The peak positions of the individual crystal planes were not affected by the prestretching process, manifesting the stable crystallite even during the stretching process. However, it is worth noting that the intensity of the strong diffraction peak at 18.6° corresponding to the 101 crystal plane decreased gradually with increasing prestretch deformation, suggesting a slight change in the internal structure of the hydrogel. The integral calculations confirmed that the prestretching treatment significantly affected the crystallinity of the material, and there was a negative correlation between the crystallinity of the material and the prestretching deformation (Figures S10 and S11). Distinctly, the 1D scattering intensity distribution profile in the equatorial direction displayed a distinct peak around 0.7 nm^{-1}, and the intensity became progressively stronger with the increase of the prestretching deformation (Figure 5a and Figure S12). It is validated that the periodic molecular bundles were presented inside the hydrogel, and the prestretching process could promote the formation of the molecular bundle.[49] In addition, the effect of prestretching treatment on the long period of lamellar crystals (L) was analyzed using Bragg's law, $L = 2\pi/q_{max}$. It is easily noticeable from Figure 5b that the long period of the material crystal increased from 8.46 to ~10 nm. It is indicated that the coiled molecular chains between the lamellar crystals perpendicular to the stretching direction formed partially by the freezing action were straightened under the prestretching effect, which in turn led to the changes in mutual distances and long periods of lamellar crystals (Figure 5c).[50,51]

The biocompatibility of the as-developed fully swollen S/PVA/1CNF/100 hydrogel was assessed in light of its promising application as an artificial ligament. Cell survival

https://doi.org/10.1021/acsnano.3c01976
ACS Nano 2023, 17, 13522−13532

and growth status are two of the most important indicators to evaluate the biocompatibility of materials. Here, human umbilical vein endothelial cells (HUVECs) were evaluated for cell morphology, live/dead double staining, and proliferative capacity. According to ISO 10993-12, we seeded HUVECs on hydrogels and selected PBS buffer as a blank control (Figure 6a). After 72 h, the morphology of the HUVECs on the hydrogel was spread widely, displaying visible actin filaments with angular structures that spread laterally with distinct cytoplasmic extensions. The cell morphologies of the hydrogels were almost the same as those of the control group (Figure 6b). Viability observations showed that only a few dead cells could be detected on the surface of the hydrogel, which was consistent with the phenomenon observed on the blank control substrate (Figure 6c). These results clearly suggested that the hydrogel did not have an adverse impact on cell growth, namely, a very limited cell toxicity.[52,53] Further, the swollen hydrogel was implanted into the subcutaneous tissue of KM mice to evaluate the organism's rejection and inflammatory response to the sample (Figure 6d,e). As can be seen in Figure 6f, even after 21 days of breeding, no abnormal inflammatory reactions, including dysplasia and necrosis, were observed in the subcutaneous tissues of KM mice surrounding the hydrogel. Further, the results of tissue section analysis (hematoxylin and eosin (H&E) stained) showed no significant changes in the mice tissue structure after 21 days, and no obvious neutrophils and lymphocytes that were common in injured tissues were found, which coincided with the experimental phenomenon in the blank control group and implied a good state of tissue health (Figure 6g). The above analysis strongly demonstrated the ideal biocompatibility of the S/PVA/1CNF/100 hydrogels and their promising prospects for application in the field of tissue engineering.

CONCLUSIONS

In summary, we demonstrated a natural-wood-inspired comprehensive strategy of prestretching−salting-out fixation to successfully complete the preparation of ultrahigh strength and supertough hybrid hydrogels with oriented structures. Due to the anisotropic structure and dense bundles of molecular fibers, the optimized oriented PVA/CNF hydrogels showed a surprising tensile strength of ∼40 MPa, an excellent longitudinal elastic modulus of 30 MPa, and an incredible toughness of over 60 MJ·m^{-3}, with overall mechanical properties superior to those of most of the strong hydrogels that have been reported so far. Moreover, the tightly arranged molecular fiber bundles could be retained after sufficient swelling and endowed the swollen samples with a breaking strength of close to 10 MPa and a toughness of 25 MJ·m^{-3}. *In vitro*, the swollen PVA/CNF hybrid hydrogel showed ideal nontoxicity and did not inhibit cell proliferation and differentiation at all. *In vivo*, the swollen hybrid hydrogel had a perfect histocompatibility. This hydrogel, with outstanding mechanical properties and good biocompatibility, offers widespread applications in the field of biological tissue engineering (e.g., artificial ligaments). Importantly, this simple preparation method could be extended to a variety of other polymer-based hydrogels to propel the application of otherwise weak hydrogels into robotics, bioengineering, and other fields.

EXPERIMENTAL SECTION

Materials. PVA (average polymerization degree: 1750 ± 50) was purchased from Sinopharm Chemical Reagent Co., Ltd. (Shanghai, China). Sodium sulfate (99%) was purchased from Aladdin Biochemical Technology Co., Ltd. (Shanghai, China). Cellulose nanofiber (CNF) was purchased from NanoFC Technology Co., Ltd. (Zhongshan, China). All of the reagents and raw materials were used without any purification.

Preparation of Pure PVA Hydrogels. PVA was added to a round-bottom flask containing some deionized water, and a 20 wt% PVA solution was obtained after continuous stirring at 92 °C for 1.5 h. Subsequently, after centrifugation at 2000 rpm, the bubble-free PVA solution was poured into a Teflon mold. After cooling to room temperature, the mold was transferred to a freezer (−20 °C) for 6 h. Next, the mold was thawed at room temperature for 6 h to obtain pure PVA hydrogel. Finally, the PVA hydrogel was immersed in 20 wt % sodium sulfate solution to investigate the effect of soaking time on the mechanical properties of the hydrogels.

Preparation of Anisotropic PVA/CNF Hydrogels. Gelatinous CNF (solid content of 4.5 wt%) was added to deionized water and emulsified continuously in a high-speed wall breaker for 5 min (12000 rpm). Subsequently, the mixture was dispersed using an ultrasonic cell disruptor for 30 min to obtain CNF dispersions with different concentrations. Then, PVA was mixed into the CNF dispersion, followed by continuous stirring at 92 °C for 1.5 h to ensure complete dissolution of the polymer, and the final PVA concentration was 20 wt %. After the air bubbles in the system were removed by a centrifugal process (2000 rpm, 2 min), the clear mixture was poured into a Teflon mold and kept at −20 °C for 6 h. Subsequently, the frozen hydrogel was thawed at room temperature for 6 h to form a preliminary PVA/CNF hydrogel. The obtained PVA/CNF hydrogels were prestretched to different tensile deformations and subsequently immersed in a 20 wt% sodium sulfate solution at 30 °C for 24 h to obtain preoriented PVA/CNF hydrogels. In term of the CNF content x (x = 0, 0.2, 0.4, 0.6, 0.8, 1, 1.2 wt%) and prestretching deformation of y (y = 0, 30, 60, 100%), the as-obtained samples were denoted as PVA/xCNF/y, as listed in Table S1. The as-obtained PVA/xCNF/y hydrogels were immersed in sufficient deionized water for 24 h; the deionized water was changed every 6 h to ensure that the hydrogels could undergo adequate ion exchange and sufficient swelling. Finally the swollen preoriented PVA/xCNF/y hydrogels were obtained and named S/PVA/xCNF/y.

Characterization. The chemical structure of the sample was analyzed by a Fourier transform infrared (FTIR) spectrometer (EQUINOX55, Bruker, Germany) in the region of 4000−600 cm^{-1}. The mechanical behavior of the sample was evaluated by an electronic tensile testing machine (Dongri, China). Test specimens were cut into dog-bone shapes and tested at a constant tension speed of 50 mm·min^{-1}. For mechanical defect testing, the sample notch width was 25% of the sample width. The microstructure images were taken with a scanning electron microscope (SEM) (Quanta 200F, FEI, USA) and transmission electron microscope (TEM) (HT7700, Hitachi, Japan).

2D small-angle X-ray scattering (2D SAXS) and 2D wide-angle X-ray diffraction (2D WAXD) patterns were collected by a Rigaku small-angle X-ray scattering system (NANOPIX, Rigaku, Japan), and the test distances for SAXS and WAXD experiments were 1803 and 64 mm, respectively. The scattering and diffraction data were analyzed using Fit2D software. 1D scattering profiles were obtained by sector integration of the 2D SAXS and 2D WAXD pattern, and the module of the scattering vector (q) was calculated by the following formula:

$$q = \frac{4\pi \sin\theta}{\lambda}$$

where λ is the X-ray wavelength (0.154 nm) and θ is the scattering angle (radian angle). From the 1D integration curve, the long period of the lamella (L) inside the material could be calculated on the basis of Bragg's law:

$$L = \frac{2\pi}{q_{max}}$$

where q_{max} is the value of q at the maximum scattering intensity.

https://doi.org/10.1021/acsnano.3c01976
ACS Nano 2023, 17, 13522−13532

Biocompatibility Evaluation. Biocompatibility was evaluated according to the following methods. Approximately 1×10^4 HUVECs/mL were seeded onto the hydrogels for 72 h. Then samples were rinsed twice in PBS buffer and fixed in 4% paraformaldehyde at room temperature for 15 min. Samples were then permeabilized in 0.5% Triton X-100 for 5 min, washed three times in PBS buffer, and stained with FITC-phalloidin (ab235137, Abcam, UK) for 30 min and 4′,6-diamidino-2-phenylindole for a further 5 min in the dark. FITC-phalloidin (red) and nuclei (blue) on scaffolds were examined using fluorescence microscopy (Olympus, Japan). HUVECs were seeded on the hydrogel at 1×10^4 cells/mL and incubated for 24 h. Cell cytotoxicity on the hydrogel was detected using a live/dead double-staining kit (KeyGen, China). Cells were stained with 2 μm calcein-AM and 8 μm propidium iodide (PI) for 15 min. Live cells were green by calcein-AM staining, whereas dead cells were red from PI staining. Stained specimens were observed and imaged using fluorescence microscopy (Leica, Germany). The inflammation test was conducted by implanting the hydrogels into subcutaneous back tissue of anesthetized KM mice. All animal studies were approved by the Animal Care and Use Committee of China Medical University (IACUC-2022099). Animals were sacrificed at 21 days postsurgery. The whole tissue plus hydrogel was harvested and fixed in 4% paraformaldehyde for histological analyses. After the process of dehydrating, impregnating, embedding by paraffin, and slicing, the pathological sections of each group were evaluated by H&E staining (Beyotime, China), and images were captured with a light optical microscope (Olympus, Japan).

ASSOCIATED CONTENT

Supporting Information

The Supporting Information is available free of charge at https://pubs.acs.org/doi/10.1021/acsnano.3c01976.

> Relationship between mechanical properties of hydrogels and soaking time; effect of CNF content on the mechanical properties of the preliminary PVA/CNF hydrogel; TEM images of CNF; effect of CNF content on the mechanical properties of PVA/*x*CNF/*y* hydrogels after soaking; SEM image of fracture section of the anisotropic PVA/1CNF/100 hydrogel; SEM images of PVA/*x*CNF/*y* hydrogels after different prestretching treatments; SEM image of Sakura tree wood; FTIR curves of different samples; breaking strength and modulus of anisotropic PVA/1CNF/100 hydrogels; XRD curves of different samples; effect of prestretching deformation variables on gel crystallization properties; 1D slices of the 2D SAXS patterns; and raw material composition of the different PVA/*x*CNF/*y* hydrogels (PDF)

AUTHOR INFORMATION

Corresponding Author

Zhong-Shuai Wu − *State Key Laboratory of Catalysis, Dalian Institute of Chemical Physics, Chinese Academy of Sciences, Dalian 116023, China; Dalian National Laboratory for Clean Energy, Dalian Institute of Chemical Physics, Chinese Academy of Sciences, Dalian 116023, China;* orcid.org/0000-0003-1851-4803; Email: wuzs@dicp.ac.cn

Authors

Lu Wu − *State Key Laboratory of Catalysis, Dalian Institute of Chemical Physics, Chinese Academy of Sciences, Dalian 116023, China*

Yue Kang − *Department of Breast Surgery, Cancer Hospital of China Medical University, Shenyang 110042, China*

Xiaoyu Shi − *State Key Laboratory of Catalysis, Dalian Institute of Chemical Physics, Chinese Academy of Sciences, Dalian 116023, China*

Bin Yuezhen − *Department of Polymer Science and Engineering, School of Chemical Engineering, Dalian University of Technology, Dalian 116024, China;* orcid.org/0000-0002-3188-721X

Meijie Qu − *Department of Polymer Science and Engineering, School of Chemical Engineering, Dalian University of Technology, Dalian 116024, China*

Jianyi Li − *Department of Breast Surgery, Cancer Hospital of China Medical University, Shenyang 110042, China*

Complete contact information is available at: https://pubs.acs.org/10.1021/acsnano.3c01976

Author Contributions

‖L. Wu and Y. Kang contributed equally to this work.

Notes

The authors declare no competing financial interest.

ACKNOWLEDGMENTS

This work was financially supported by the National Natural Science Foundation of China (22125903, 51872283, 22109160), Dalian Innovation Support Plan for High Level Talents (2019RT09), Dalian National Laboratory For Clean Energy (DNL), CAS, DNL Cooperation Fund, CAS (DNL202016, DNL202019), DICP (DICP I2020032), the Joint Fund of the Yulin University and the Dalian National Laboratory for Clean Energy (YLU-DNL Fund 2021002, YLU-DNL Fund 2021009), and the China Postdoctoral Science Foundation (2021M693126).

REFERENCES

(1) Le, X. X.; Lu, W.; Zhang, J. W.; Chen, T. Recent Progress in Biomimetic Anisotropic Hydrogel Actuators. *Adv. Sci.* **2019**, *6* (5), No. 1801584.

(2) Cui, Y. D.; Li, D.; Gong, C.; Chang, C. Y. Bioinspired Shape Memory Hydrogel Artificial Muscles Driven by Solvents. *ACS Nano* **2021**, *15* (8), 13712−13720.

(3) Wei, P. L.; Chen, T.; Chen, G. Y.; Hou, K.; Zhu, M. F. Ligament-Inspired Tough and Anisotropic Fibrous Gel Belt with Programed Shape Deformations via Dynamic Stretching. *ACS Appl. Mater. Interfaces* **2021**, *13* (16), 19291−19300.

(4) Rana, H. H.; Park, J. H.; Gund, G. S.; Park, H. S. Highly conducting, extremely durable, phosphorylated cellulose-based ionogels for renewable flexible supercapacitors. *Energy Storage Mater.* **2020**, *25*, 70−75.

(5) Gund, G. S.; Park, J. H.; Harpalsinh, R.; Kota, M.; Shin, J. H.; Kim, T. I.; Gogotsi, Y.; Park, H. S. MXene/Polymer Hybrid Materials for Flexible AC-Filtering Electrochemical Capacitors. *Joule* **2019**, *3* (1), 164−176.

(6) Dong, Q.; Zhang, X.; Qian, J.; He, S. M.; Mao, Y. M.; Brozena, A. H.; Zhang, Y.; Pollard, T. P.; Borodin, O. A.; Wang, Y. B.; Chava, B. S.; Das, S.; Zavalij, P.; Segre, C. U.; Zhu, D. Y.; Xu, L.; Liang, Y. L.; Yao, Y.; Briber, R. M.; Li, T.; Hu, L. B. A Cellulose-derived Supramolecule for Fast Ion Transport. *Sci. Adv.* **2022**, *8* (49), No. eadd2031.

(7) Xu, L.; Meng, T. T.; Zheng, X. Y.; Li, T. Y.; Brozena, A. H.; Mao, Y. M.; Zhang, Q.; Clifford, B. C.; Rao, J. C.; Hu, L. B. Nanocellulose-Carboxymethylcellulose Electrolyte for Stable, High-Rate Zinc-Ion Batteries. *Adv. Funct. Mater.* **2023**, *33*, 2302098.

(8) Wu, M. L.; Zhang, Y.; Xu, L.; Yang, C. P.; Hong, M.; Cui, M. J.; Clifford, B. C.; He, S. M.; Jing, S. S.; Yao, Y.; Hu, L. B. A Sustainable Chitosan-Zinc Electrolyte for High-Rate Zinc-Metal Batteries. *Matter* **2022**, *5* (10), 3402−3416.

(9) Kong, W. Q.; Wang, C. W.; Jia, C.; Kuang, Y. D.; Pastel, G.; Chen, C. J.; Chen, G. G.; He, S. M.; Huang, H.; Zhang, J. H.; Wang, S.; Hu, L. B. Muscle-Inspired Highly Anisotropic, Strong, Ion-Conductive Hydrogels. *Adv. Mater.* **2018**, *30* (39), No. 1801934.
(10) Itagaki, H.; Kurokawa, T.; Furukawa, H.; Nakajima, T.; Katsumoto, Y.; Gong, J. P. Water-Induced Brittle-Ductile Transition of Double Network Hydrogels. *Macromolecules* **2010**, *43* (22), 9495−9500.
(11) Zhang, Y. K.; Xue, J. J.; Li, D. P.; Li, H. Y.; Huang, Z. H.; Huang, Y. W.; Gong, C. J.; Long, S. J.; Li, X. F. Tough Hydrogels with Tunable Soft and Wet Interfacial Adhesion. *Polym. Test.* **2021**, *93*, No. 106976.
(12) Wu, S.; Lou, D. Y.; Wang, H. Y.; Jiang, D. Q.; Fang, X.; Meng, J. Q.; Sun, X. Y.; Li, J. One-pot Synthesis of Anti-freezing Carrageenan/polyacrylamide Double-network Hydrogel Electrolyte for Low-temperature Flexible Supercapacitors. *Chem. Eng. J.* **2022**, *435* (2), No. 135057.
(13) Zhao, L. M.; Zhang, J.; Cao, P.; Kang, L. X.; Gong, Q.; Wang, J. J.; Zhang, Y. Y.; Li, Q. W. Fast Water Transport Reversible CNT/PVA Hybrid Hydrogels with Highly Environmental Tolerance for Multifunctional Sport Headband. *Compos. Part B-Eng.* **2021**, *211*, No. 108661.
(14) Chen, C. C.; Wang, Y. R.; Zhou, T.; Wan, Z. M.; Yang, Q. L.; Xu, Z. Y.; Li, D. G.; Jin, Y. C. Toward Strong and Tough Wood-Based Hydrogels for Sensors. *Biomacromolecules* **2021**, *22* (12), 5204−5213.
(15) Wang, Z. Q.; Cheng, F. C.; Cai, H. C.; Li, X. R.; Sun, J. P.; Wu, Y. Q.; Wang, N. N.; Zhu, Y. Q. Robust Versatile Nanocellulose/Polyvinyl Alcohol/Carbon Dot Hydrogels for Biomechanical Sensing. *Carbohydr. Polym.* **2021**, *259*, No. 117753.
(16) Chen, C. J.; Kuang, Y. D.; Zhu, S. Z.; Burgert, I.; Keplinger, T.; Gong, A.; Li, T.; Berglund, L.; Eichhorn, S. J.; Hu, L. B. Structure-Property-Function Relationships of Natural and Engineered Wood. *Nat. Rev. Mater.* **2020**, *5* (9), 642−666.
(17) Song, J. W.; Chen, C. J.; Zhu, S. Z.; Zhu, M. W.; Dai, J. Q.; Ray, U.; Li, Y. J.; Kuang, Y. D.; Li, Y. F.; Quispe, N.; Yao, Y. G.; Gong, A.; Leiste, U. H.; Bruck, H. A.; Zhu, J. Y.; Vellore, A.; Li, H.; Minus, M. L.; Jia, Z.; Martini, A.; Li, T.; Hu, L. B. Processing Bulk Natural Wood into a High-performance Structural Material. *Nature* **2018**, *554* (7691), 224−228.
(18) Gustavsson, L.; Sathre, R. Variability in Energy and Carbon Dioxide Balances of Wood and Concrete Building Materials. *Build Environ.* **2006**, *41* (7), 940−951.
(19) Berglund, L. A.; Burgert, I. Bioinspired Wood Nanotechnology for Functional Materials. *Adv. Mater.* **2018**, *30* (19), No. 1704285.
(20) Yu, Z. L.; Qin, B.; Ma, Z. Y.; Gao, Y. C.; Guan, Q. F.; Yang, H. B.; Yu, S. H. Emerging Bioinspired Artificial Woods. *Adv. Mater.* **2021**, *33* (28), No. 2001086.
(21) Culver, H. R.; Clegg, J. R.; Peppas, N. A. Analyte-Responsive Hydrogels: Intelligent Materials for Biosensing and Drug Delivery. *Acc. Chem. Res.* **2018**, *51* (10), 2600−2600.
(22) Boote, C.; Dennis, S.; Huang, Y. F.; Quantock, A. J.; Meek, K. M. Lamellar Orientation in Human Cornea in Relation to Mechanical Properties. *J. Struct. Biol.* **2005**, *149* (1), 1−6.
(23) Liu, K.; Han, L.; Tang, P.; Yang, K.; Gan, D.; Wang, X.; Wang, K.; Ren, F.; Fang, L.; Xu, Y.; Lu, Z.; Lu, X. An Anisotropic Hydrogel Based on Mussel-Inspired Conductive Ferrofluid Composed of Electromagnetic Nanohybrids. *Nano Lett.* **2019**, *19* (12), 8343−8356.
(24) Nie, J. Y.; Pei, B. Y.; Wang, Z. K.; Hu, Q. L. Construction of Ordered Structure in Polysaccharide Hydrogel: A Review. *Carbohydr. Polym.* **2019**, *205*, 225−235.
(25) Wang, X. F.; Fang, J.; Zhu, W. W.; Zhong, C. X.; Ye, D. D.; Zhu, M. Y.; Lu, X.; Zhao, Y. S.; Ren, F. Z. Bioinspired Highly Anisotropic, Ultrastrong and Stiff, and Osteoconductive Mineralized Wood Hydrogel Composites for Bone Repair. *Adv. Funct. Mater.* **2021**, *31* (20), No. 2010068.
(26) Yan, G. H.; He, S. M.; Chen, G. F.; Ma, S.; Zeng, A. Q.; Chen, B. L.; Yang, S. L.; Tang, X.; Sun, Y.; Xu, F.; Lin, L.; Zeng, X. H. Highly Flexible and Broad-Range Mechanically Tunable All-Wood Hydrogels with Nanoscale Channels via the Hofmeister Effect for Human Motion Monitoring. *Nano-Micro Lett.* **2022**, *14* (1), 84.
(27) Chen, G. G.; Li, T.; Chen, C. J.; Kong, W. Q.; Jiao, M. L.; Jiang, B.; Xia, Q. Q.; Liang, Z. Q.; Liu, Y.; He, S. M.; Hu, L. B. Scalable Wood Hydrogel Membrane with Nanoscale Channels. *ACS Nano* **2021**, *15* (7), 11244−11252.
(28) Li, J.; Chee, H. L.; Chong, Y. T.; Chan, B. Q. Y.; Xue, K.; Lim, P. C.; Loh, X. J.; Wang, F. K. Hofmeister Effect Mediated Strong PHEMA-Gelatin Hydrogel Actuator. *ACS Appl. Mater. Interfaces* **2022**, *14* (20), 23826−23838.
(29) Zhang, Y. J.; Cremer, P. S. Interactions Between Macromolecules and Ions: The Hofmeister Series. *Curr. Opin. Chem. Biol.* **2006**, *10* (6), 658−663.
(30) Yang, X. P.; Abe, K.; Biswas, S. K.; Yano, H. Extremely Stiff and Strong Nanocomposite Hydrogels with Stretchable Cellulose Nanofiber/Poly(vinyl alcohol) Networks. *Cellulose* **2018**, *25* (11), 6571−6580.
(31) Jungwirth, P.; Cremer, P. S. Beyond Hofmeister. *Nat. Chem.* **2014**, *6* (4), 261−263.
(32) Wang, S. N.; Chen, H.; Li, K.; Koskela, S.; Berglund, L. A.; Zhou, Q. Strong, Transparent, and Thermochromic Composite Hydrogel from Wood Derived Highly Mesoporous Cellulose Network and PNIPAM. *Compos. Part A-Appl. S.* **2022**, *154*, No. 106757.
(33) Li, X. F.; Shang, L. L.; Li, D. P.; Wang, W.; Chen, S. L.; Zhong, H. W.; Huang, Y. W.; Long, S. J. High-Strength, Strong-Adhesion, and Antibacterial Polyelectrolyte Complex Hydrogel Films from Natural Polysaccharides. *Polym. Test.* **2022**, *109*, No. 107547.
(34) Yang, F. C.; Zhao, J. C.; Koshut, W. J.; Watt, J.; Riboh, J. C.; Gall, K.; Wiley, B. J. A Synthetic Hydrogel Composite with the Mechanical Behavior and Durability of Cartilage. *Adv. Funct. Mater.* **2020**, *30* (36), No. 2003451.
(35) Zhang, M. H.; Chen, S. Y.; Sheng, N.; Wang, B. X.; Wu, Z. T.; Liang, Q. Q.; Wang, H. P. Anisotropic Bacterial Cellulose Hydrogels with Tunable High Mechanical Performances, Non-Swelling and Bionic Nanofluidic Ion Transmission Behavior. *Nanoscale* **2021**, *13* (17), 8126−8136.
(36) Mredha, M. T. I.; Le, H. H.; Tran, V. T.; Trtik, P.; Cui, J. X.; Jeon, I. Anisotropic Tough Multilayer Hydrogels with Programmable Orientation. *Mater. Horiz.* **2019**, *6* (7), 1504−1511.
(37) He, Q. Y.; Huang, Y.; Wang, S. Y. Hofmeister Effect-Assisted One Step Fabrication of Ductile and Strong Gelatin Hydrogels. *Adv. Funct. Mater.* **2018**, *28* (5), No. 1705069.
(38) Li, F. B.; Zhang, G. Z.; Wang, Z. S.; Jiang, H. Y.; Feng, X. Q.; Yan, S.; Zhang, L.; Li, H. J.; Zhao, T. Y.; Liu, M. J. Bioinspired Nonswellable Ultrastrong Nanocomposite Hydrogels with Long-Term Underwater Superoleophobic Behavior. *Chem. Eng. J.* **2019**, *375*, No. 122047.
(39) Yao, B.; Yan, Y.; Cui, Q.; Duan, S.; Wang, C.; Du, Y.; Zhao, Y.; Wu, D.; Wu, S.; Zhu, X.; Hsiai, T.; He, X. Ultrastrong, Highly Conductive and Capacitive Hydrogel Electrode for Electron-ion Transduction. *Matter* **2022**, *5*, 4407−4424.
(40) Cai, Y. Q.; Shi, J. C.; Liu, F. Z.; Li, H. C.; Man, X. Y.; Guan, S. Hofmeister Effect-Assisted Strong Natural Biopolymer-Based Hydrogels with Multi-Functions. *Chin. J. Chem.* **2021**, *39* (11), 3085−3092.
(41) Zhang, Y.; Ye, L. Structure and Property Of Polyvinyl Alcohol/Precipitated Silica Composite Hydrogels for Microorganism Immobilization. *Compos. Part B-Eng.* **2014**, *56*, 749−755.
(42) Hu, J. Q.; Wu, Y. L.; Yang, Q.; Zhou, Q. W.; Hui, L. F.; Liu, Z.; Xu, F.; Ding, D. Y. One-pot Freezing-Thawing Preparation of Cellulose Nanofibrils Reinforced Polyvinyl Alcohol Based Ionic Hydrogel Strain Sensor for Human Motion Monitoring. *Carbohydr. Polym.* **2022**, *275*, No. 118697.
(43) Wang, H. Q.; Fang, S. Q.; Zuo, M.; Li, Z.; Yu, X.; Tang, X.; Sun, Y.; Yang, S. L.; Zeng, X. H.; Lin, L. Removal of Copper Ions by Cellulose Nanocrystal-Based Hydrogel and Reduced Adsorbents for Its Catalytic Properties. *Cellulose* **2022**, *29* (8), 4525−4537.
(44) Paduraru, O. M.; Ciolacu, D.; Darie, R. N.; Vasile, C. Synthesis and Characterization of Polyvinyl Alcohol/Cellulose Cryogels and

https://doi.org/10.1021/acsnano.3c01976
ACS Nano 2023, 17, 13522−13532

Their Testing as Carriers for A Bioactive Component. *Mater. Sci. Eng. C-Mater.* **2012**, *32* (8), 2508−2515.
(45) Xiang, C. P.; Wang, Z. J.; Yang, C. H.; Yao, X.; Wang, Y. C.; Suo, Z. G. Stretchable and Fatigue-Resistant Materials. *Mater. Today* **2020**, *34*, 7−16.
(46) Hua, M. T.; Wu, S. W.; Ma, Y. F.; Zhao, Y. S.; Chen, Z. L.; Frenkel, I.; Strzalka, J.; Zhou, H.; Zhu, X. Y.; He, X. M. Strong Tough Hydrogels via the Synergy of Freeze-Casting and Salting Out. *Nature* **2021**, *590* (7847), 594−599.
(47) Duan, T. C.; Xu, H. J.; Tang, Y. J.; Jin, J.; Wang, Z. B. Effect of Epitaxial Crystallization on The Structural Evolution of PCL/RGO Nanocomposites During Stretching by In-Situ Synchrotron Radiation. *Polymer* **2018**, *159*, 106−115.
(48) Paranhos, C. M.; Soares, B. G.; Oliveira, R. N.; Pessan, L. A. Poly(vinyl alcohol)/clay-Based Nanocomposite Hydrogels: Swelling Behavior and Characterization. *Macromol. Mater. Eng.* **2007**, *292* (5), 620−626.
(49) Zhang, R.; Zhang, Q. L.; Ji, Y. X.; Su, F. M.; Meng, L. P.; Qi, Z. M.; Lin, Y. F.; Li, X. Y.; Chen, X. W.; Lv, F.; Li, L. B. Stretch-induced Complexation Reaction Between Poly(vinyl alcohol) and Iodine: An In Situ Synchrotron Radiation Small- and Wide-Angle X-Ray Scattering Study. *Soft Matter* **2018**, *14* (13), 2535−2546.
(50) Brown, H. R.; Kramer, E. J. Craze Microstructure from Small-Angle X-Ray-Scattering (Saxs). *J. Macromol. Sci. Phys.* **1981**, *B19* (3), 487−522.
(51) Liu, L. Z.; Hsiao, B. S.; Fu, B. X.; Ran, S. F.; Toki, S.; Chu, B.; Tsou, A. H.; Agarwal, P. K. Structure Changes During Uniaxial Deformation of Ethylene-Based Semicrystalline Ethylene-Propylene Copolymer. 1. SAXS study. *Macromolecules* **2003**, *36* (6), 1920−1929.
(52) Li, Y. Q.; Yu, T.; Yang, T. Y.; Zheng, L. X.; Liao, K. Bio-Inspired Nacre-like Composite Films Based on Graphene with Superior Mechanical, Electrical, and Biocompatible Properties. *Adv. Mater.* **2012**, *24* (25), 3426−3431.
(53) Liu, L.; Zhu, M. H.; Xu, X. D.; Li, X.; Ma, Z. W.; Jiang, Z.; Pich, A.; Wang, H.; Song, P. A. Dynamic Nanoconfinement Enabled Highly Stretchable and Supratough Polymeric Materials with Desirable Healability and Biocompatibility. *Adv. Mater.* **2021**, *33* (51), No. 2105829.

https://doi.org/10.1021/acsnano.3c01976
ACS Nano 2023, 17, 13522−13532